The Novel Oxy-sulfide Glassy Ionic Conductors $Na_4P_2S_{7-x}O_x \ 0 \le x \le 7$: Understanding the Features of Static and Dynamic Cations

Ananda Shastri *,1 , Nathan Rons 1 , Qing-Ping Ding 2 , Stephen J. Kmiec 3 , Madison Olson 3 , 1	Yuji
Furukawa ^{2,4} , Steve W. Martin ^{2,3}	

¹Department of Physics and Astronomy, Minnesota State University Moorhead, Moorhead, MN 56560, USA

²Ames Laboratory, U.S. Department of Energy, Iowa State University, Ames, IA 50011, USA

³Department of Materials Science and Engineering, Iowa State University, Ames, IA 50011,

USA

⁴Department of Physics and Astronomy, Iowa State University, Ames, IA 50011, USA

*Corresponding author: shastri@mnstate.edu, 218 477 2448

Abstract

We present a ²³Na nuclear spin dynamics model for interpreting nuclear magnetic resonance (NMR) spin-lattice relaxation and central linewidth data in the invert glass system $Na_4P_2S_{7-x}O_x$, $0 \le x \le 7$. The glassy nature of this material results in variations in local Na^+ cation environments that may be described by a Gaussian distribution of activation energies. A consistent difference between the mean activation energies determined by NMR and DC conductivity measurements was observed, and interpreted using a percolation theory model. From this, the Na-Na coordination number in the sodium cation sublattice was obtained. These values were consistent with jumps through tetrahedral faces of the sodium cages for the sulfur rich glasses, x < 5, consistent with proposed models of their short range order (SRO) structures. From NMR spin-echo measurements, we determined the Na-Na second moment M₂ resulting from the Na-Na magnetic dipole interaction of nearest neighbors. Values of M₂ obtained as a function of sodium number density N were in agreement with models for uniform sodium distribution, indicating that these invert glass systems form so as to maximize the average Na-Na distance. A simple Coulombic attraction model between Na⁺ cation and X (=S⁻, O⁻) anion was applied to calculate the activation energy. In the range $1.5 \le x \le 7$, an increase in activation energy with increasing oxygen content x occurred, and was consistent with the decrease in average anionic radius, and thus increasing the Coulombic attraction. For small oxygen additions, $0 \le x \le 1.5$, however, the model was not consistent with a local minimum in te activation energy as suggested by DC conductivity data. This minimum has been attributed to a localized expansion in the volume available for the Na⁺ diffusion that leads to a decrease in the volumetric strain part of the conductivity activation energy.

I. Introduction

Sodium solid state batteries (SSSB) are an attractive solution to the problem of electrical grid-scale energy storage for renewable energy sources, such as solar and wind farms [1]. However, because sodium batteries currently implement a highly flammable liquid electrolyte, it is desirable to develop a non-flammable solid-state electrolyte (SSE) for sodium battery applications. Glasses have been considered viable SSEs for decades [2], and possess several properties that make them suitable candidates: high DC ionic conductivity, intrinsic lack of grain boundaries, and scalable processing methods [3]. Glasses have a structural framework that has a higher configurational entropy than that of the corresponding crystal, resulting in larger free volume within the material for potential interstitial ionic sites [4]. To be useful in battery applications, a SSE must have a conductivity on the order of 10⁻⁴ S/cm. A decade ago, investitaion of the Na₂S + P₂S₅ system resulted in glass-ceramics with room temperature conductivities of 5 x 10^{-4} S/cm [5], but these lacked stability with sodium electrodes, a recurring problem in sulfide-based systems. In contrast, oxide glasses are highly stable, but many years of work on these systems has yielded conductivities that are still too low for a useful SSE. Mixed oxy-sulfide (MOS) glass systems can maximize conductivity and stability by finding an optimal combination of oxygen and sulfur. Additionally, adding oxygen in low concentrations can increase the ionic conducitivity of a MOS glass by up to an order of magnitude, an effect attributed to increasing the free volume within the structure [6].

Our group recently reported on the melt-quenched $yNa_2S + (1-y)P_2S_{7-x}O_x$ invert glass series with oxygen content $0 \le x \le 7$, and the molar fraction of network modifier 0.5 < y < 0.75. For invert glasses, the glass network consists of relatively short chains of corner-sharing polyhedral[4]. In this case, the short-range order (SRO) structures are P-centered tetrahedral. Anions at the corners may be shared with other tetrahedral to form a bridging anion site (BX, where X = S, O). Alternatively, a site may be a non-bridging anion site (NBX), and instead form an ionic bond with the Na+ cations. For charge balancing, the number of NBX is equal to the number of cations in the structure. The high molar fraction y of network modifier Na₂S thus prevents the SRO from creating an extended structure, and results in relatively short polymer chains.

In particular, we have recently prepared and characterized the y=0.67 (Na₄P₂S_{7-x}O_x) glass series [7]. The structure is indicated schematically in Fig. 1. As the oxygen content changes from 0 to 7, the sodium number density N changes slowly from1.27 x 10^{28} m⁻³ to 2.29 x 10^{28} m⁻³ [8]. The room-temperature DC conductivity reaches a maximum of ~3x 10^{-6} (Ω cm)⁻¹ for dilute oxygen content x ~ 0.5, falling two orders of magnitude as x increases across the composition range [8]. The activation energy to ionic motion Δ Eact was obtained from DC conductivity measurements. Further, the glassy state of this system results in a distribution of Coulombic traps of varying strengths. As a result, some Na⁺ are expected to reside in particular deep traps and may therefore be considered as essentially static and rigidly connected to the glass network. These form part of the structure around which ionic diffusion occurs. Other Na⁺ cations are expected to be found at the other end of the distribution in shallow traps, and therefore serve as charge carriers for ionic motion. In

between these two extremes lies the vast majority of the Na⁺ cations whose contribution to the Na⁺ ionic current depends upon the depth of the particular trap of the Na⁺.

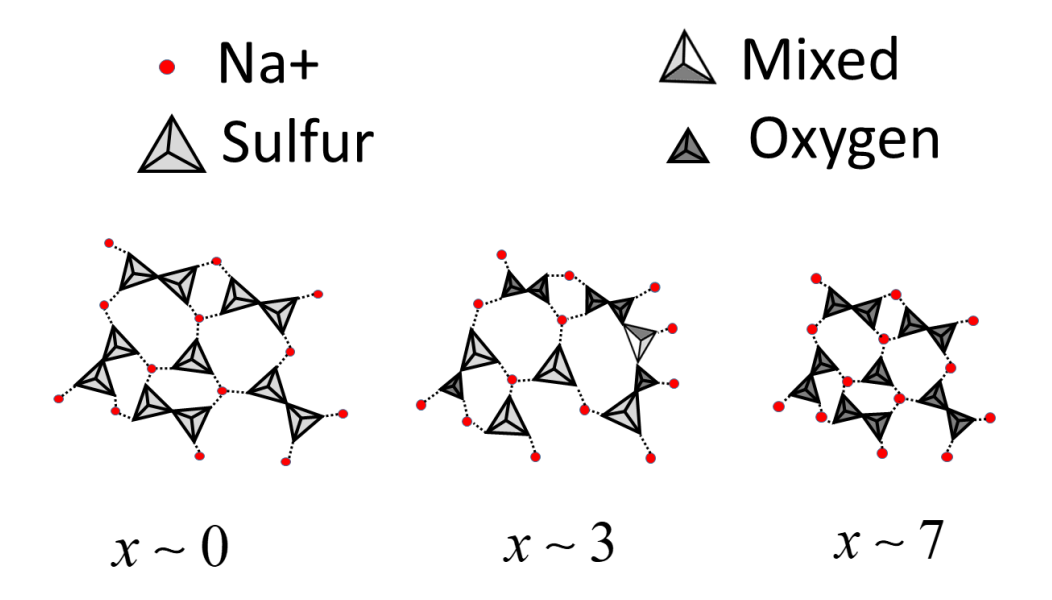


FIGURE 1. Two-dimensional, schematic representation of Na₄P₂S_{7-x}O_x glass structures for different oxygen content x values. The figure indicates the approximate length of SRO chains and the approximate distribution of SRO units [7], and suggests the variation in size of the SRO structures. Circles represent the Na⁺ cation; uniformly shaded tetrahedral represent SRO structures with all vertices occupied by the same atomic species, either sulfur or oxygen; and tetrahedral with mixed shading represent SRO structures with a mixture of oxygen and sulfur atoms at vertices. Dotted lines indicate ionic bonds.

Nuclear magnetic resonance (NMR) is a well-established tool for yielding information about local structure and dynamics of resonant nuclei [9-11]. It has been applied extensively to ²³Na nuclei in Na⁺ conducting glasses [12-17]. In glassy systems, structural information such as cation coordination number and cation distribution is essential for understanding ionic motion [12]. For ionic motion in glasses characterized by both DC conductivity and NMR, significantly different motion correlation times and activation energies are often found. This effect can be attributed to the sensitivity of the DC conductivity to ionic hopping over lower energy barriers [18,19]. Percolation theory has been applied to model ion dynamics

in various systems [18,19], and has been used to model the DC ionic conductivity in sodium invert glasses when no NMR data was available [17]. Ion distributions have been probed in dilute sodium glasses using 23 Na spin-echo methods that give access to magnetic dipoledipole interactions between nearest neighbors in the sodium sublattice [12-14]. Using $M_2(N)$ —the NMR second moment as a function of sodium number density N—as a metric for this interaction, different model distributions may be tested. In sodium glasses where N < 1.5×10^{28} m-3, simple clustering, random clustering, and uniform distributions of Na have been reported [12].

This study will show for the first time that the sodium dynamics in these glasses may be described in terms of ionic percolation over a Gaussian distribution of energy barriers. Applying percolation theory, we obtained the average number of ion channels per sodium site for the percolation network. We will show that the spatial distribution of the sodium ions is uniform, and present a model for the activation energy based on ionic interactions within the structure.

II. Experimental Methods

Glassy solid electrolytes for $Na_4P_2S_{7-x}O_x$, $0 \le x \le 7$ were prepared using the MQ techniques as described in [7] in a N_2 glovebox using as-received sodium sulfide (Na_2S 99.9% Alfa Aesar), phosphorous pentasulfide (P_2S_5 , 99.95% Sigma Aldrich), and phosphorous pentoxide (P_2O_5 , 99.95% Fisher Scientific). 2 to 3 mm thick glass samples were cast onto a preheated mold set to ~35 °C below the T_g , annealed for approximately 3 hours, and then cooled to room temperature at a rate of 1 °C/min. Samples for NMR were flame sealed in thin-walled quartz tubes under 0.16 atm pressure of helium gas.

NMR measurements were performed on ^{23}Na (nuclear spin I=3/2, gyromagnetic ratio $\gamma/2\pi$ =11.2653 MHz/T) by using a homemade phase-coherent spin-echo pulse spectrometer from 4.2 K to just below the T_g of the samples, $\sim\!500$ K.

NMR was performed on two different stations. Both were operated at nearly the same resonance condition for the 23 Na nuclei, namely B_0 =7.41 T and ν_L =83.48 MHz. All measurements from room temperature to 500 K were performed on an Oxford Systems, fixed-field, superconducting magnet fitted with a high-temperature cryostat and NMR probe built in our lab. Measurements below room temperature were performed on an adjustable-field, superconducting magnet built in-house. NMR data were obtained using computer-controlled, phase coherent, NMR spectrometers.

A. Field scans

As discussed in the Appendix, the 23 Na nucleus has an electric quadrupole moment that interacts with the local electric field gradient. We characterized this interaction for interpretation of the nuclear dynamics following our work in other sodium glasses [17]. Wide-line NMR spectra were obtained for Na₄P₂S_{7-x}O_x x = 0, 1.5, 3, 5, 7 at a temperature of 4.2 K. The magnetic field was swept at 0.0015 T/min at using a fixed radio frequency (RF) of $\nu_L=83.4766$ MHz while capturing the integrated spin-echo signal from a ($\frac{\pi}{2}|_x-20\mu s-\pi_y-20\mu s-echo$) pulse sequence with a 4-phase cycling sequence. The RF pulse width was $\tau_{\pi/2}=4\mu s$.

B. ²³Na central line NMR linewidth versus temperature

In preparation for the 23 Na motional narrowing experiments, both spectrometers were tested with 0.03 mol fraction NaCl (aq) solution at room temperature. The sample position of most uniform magnetic field was found by maximizing the duration T_2^* of the 23 Na free induction decay (FID) NMR signal of the test solution, and corresponded to a full width at half maximum (FWHM) value of 600-700 Hz. This optimal sample position was used for all subsequent line-width measurements for the sodium glasses. The temperature dependence of the FWHM of the central line ($^{-1}$ / $_2$ \leftrightarrow 1 / $_2$) was found by Fourier transforming the FID following a 4 μ s RF pulse.

C. ²³Na central line NMR spin-lattice relaxation rate versus temperature

The return to equilibrium after selective irradiation of the central line leads to multi-exponential recovery in crystalline solids [20]. In glasses, the distribution of local environments and interactions results in a stretched exponential recovery. We performed saturation recovery [21] of the 23 Na central line using the pulse sequence $comb-t-\frac{\pi}{2}\Big|_x$, where the saturating comb had a total of 5 RF pulses at intervals of 1 ms each with pulse length $\tau_{\pi/2}=20\,\mu s$. The 23 Na nuclear magnetization $M_Z(t)$ along the static field B_0 was measured as the integrated FID signal. Long-time values $M_{_{\infty}}$ were estimated by averaging the three longest t-values for which the $M_Z(t)$ appeared constant.

D. ²³Na NMR second moment

Because this technique probes the spatial distribution of 23 Na sites, we performed all measurements at 100 K, a temperature at which the 23 Na ionic motion was effectively frozen out.

Following Refs. [12,13,17], the 23 Na rigid-lattice second moment M_2 for the homonuclear magnetic dipole-dipole interaction, was obtained using a spin-echo sequence ($\frac{\pi}{2}\Big|_{x} - \tau - \pi_{y} - \tau - echo$), taking care to irradiate only the central line. The duration of the π_{y} pulse was 8 μ s. In the zero-time M_2 method (ZTMM) [13], data acquired over short spin evolution times $100~\mu$ s < 2τ < $250~\mu$ s are fit to a Gaussian function over a progressively smaller upper boundary time $2\tau_{max}$. The sequence of M_2 values may be extended to zero time using a linear extrapolation, to yield a short-time estimate of M_2 that should be sensitive to the closest—and therefore most strongly interacting—sodium nuclei [13]. To reduce the sensitivity of ZTMM to high-frequency noise components, we modified this approach by fitting a compressed exponential function [22] to the overall spin-echo. The model function was used to calculated a simulated data set over $2\tau_{min}$ < 2τ < $2\tau_{max}$ in order to implement ZTMM. See the next section for additional information.

III. Results

A. Field scans

The NMR Hamiltonian for the ²³Na nucleus, and the distributions relevant for powdered sodium glass samples, are described in detail in the Appendix. Interactions between the ²³Na nucleus and the local environment are described by the sum of Zeeman (\mathcal{H}_{Z}) , electric quadrupole (\mathcal{H}_{O}) , and magnetic dipole interactions (\mathcal{H}_{D}) . The conditions of this study, namely $\mathcal{H}_{\!\scriptscriptstyle Z} > \mathcal{H}_{\!\scriptscriptstyle O}$, result in a spectrum with a sharp central transition line (Iz=- $1/2 \leftrightarrow 1/2$) flanked by the satellite transitions ($I_z=1/2 \leftrightarrow 3/2$ and $-1/2 \leftrightarrow -3/2$) on either side. For a single crystal, this results in a central line symmetrically straddled by two quadrupole satellites. The separation of the peaks is proportional to $\nu_{\scriptscriptstyle O}$, the strength of quadrupole interaction, which is proportional to the largest electric field gradient (EFG) in the principal axis system of the EFG tensor [9,11]. Another important quantity is η , the asymmetry parameter for the EFG [9,11], which is the fractional difference of the minor gradients in the principal axis system. For a crystalline powder, the distribution in grain orientations results in features (singularities and shoulders), as shown by the simulated crystal powder pattern in Fig. 2. By comparing simulated powder patterns to field scan data, one may extract a unique v_0 and η for each non-equivalent resonant nuclear site in the crystal [23].

Figure 2 shows the ²³Na spin-echo amplitude plotted versus magnetic field for samples across the glass composition range. For clarity, the central line was not scanned for these experiments. All sample spectra exhibited a broad, essentially featureless, NMR first-order electric quadrupole satellite powder pattern. As seen in Fig. 2, the data are not

consistent with crystalline powder patterns, and are similar to patterns we have reported in other sodium glasses [17]. The width of the quadrupole satellite distribution increased as the oxygen content x increased.

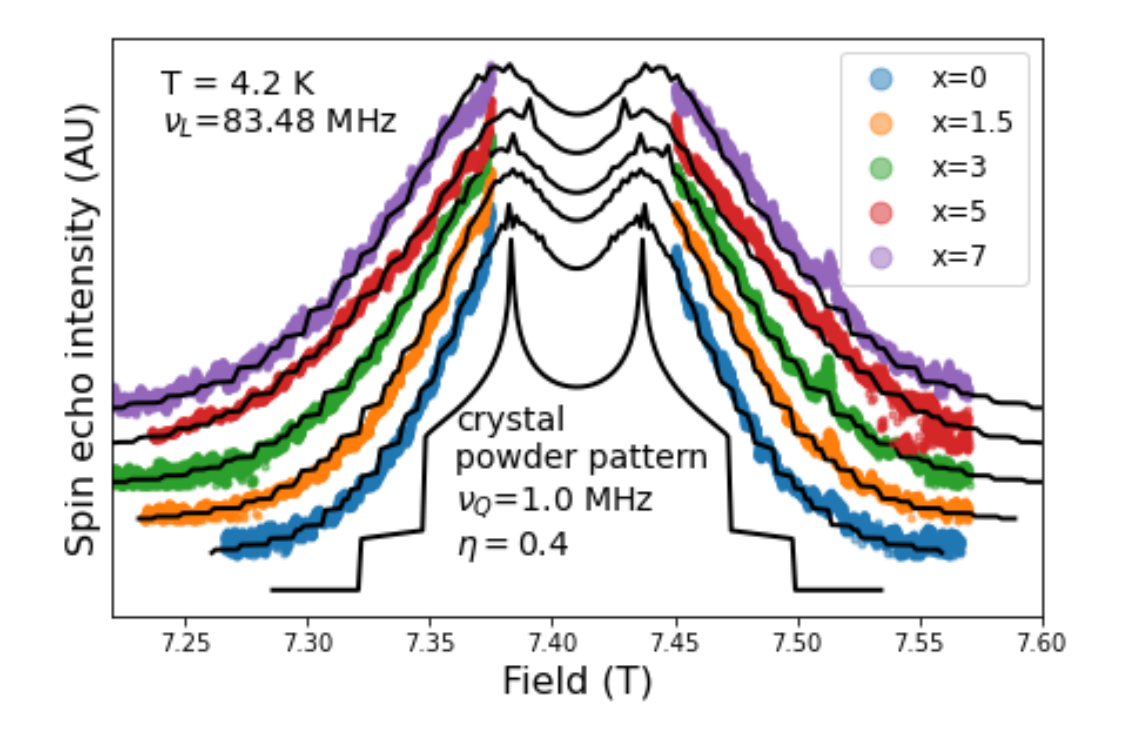


FIGURE 2. Field-swept ²³Na spin-echo amplitude versus magnetic field scans for the glass system Na₄P₂S_{7-x}O_x, where x=0, 1.5, 3, 5, and 7, taken at temperature 4.2 K and frequency ν_L =83.48 MHz. Solid lines are powder pattern simulations using a Czjzek distribution of parameters ν_Q , η , and σ_Q , as described in the Appendix. For comparison, a powder pattern for a crystal with a single value of ν_Q and η is shown. The field sweep and powder pattern do not include the central line.

We simulated the NMR field scan data as a powder pattern of the first-order electric quadrupole interaction. The glassy nature of the material [24] was simulated by assuming a Cjzjek distribution $P(\nu_Q,\eta)$ of crystalline powder patterns of width σ_Q (see Appendix). Figure 2 shows the simulated spectra as solid lines. Given the lack of distinct features in the

NMR spectrum, we performed multiple simulations for each glass composition to explore the extent of parameter variation yielding simulations in agreement with the data. Values of v_{ϱ} , η , and σ_{ϱ} were averaged, and the results are plotted in Fig. 3, where the error bars indicated the standard deviation.

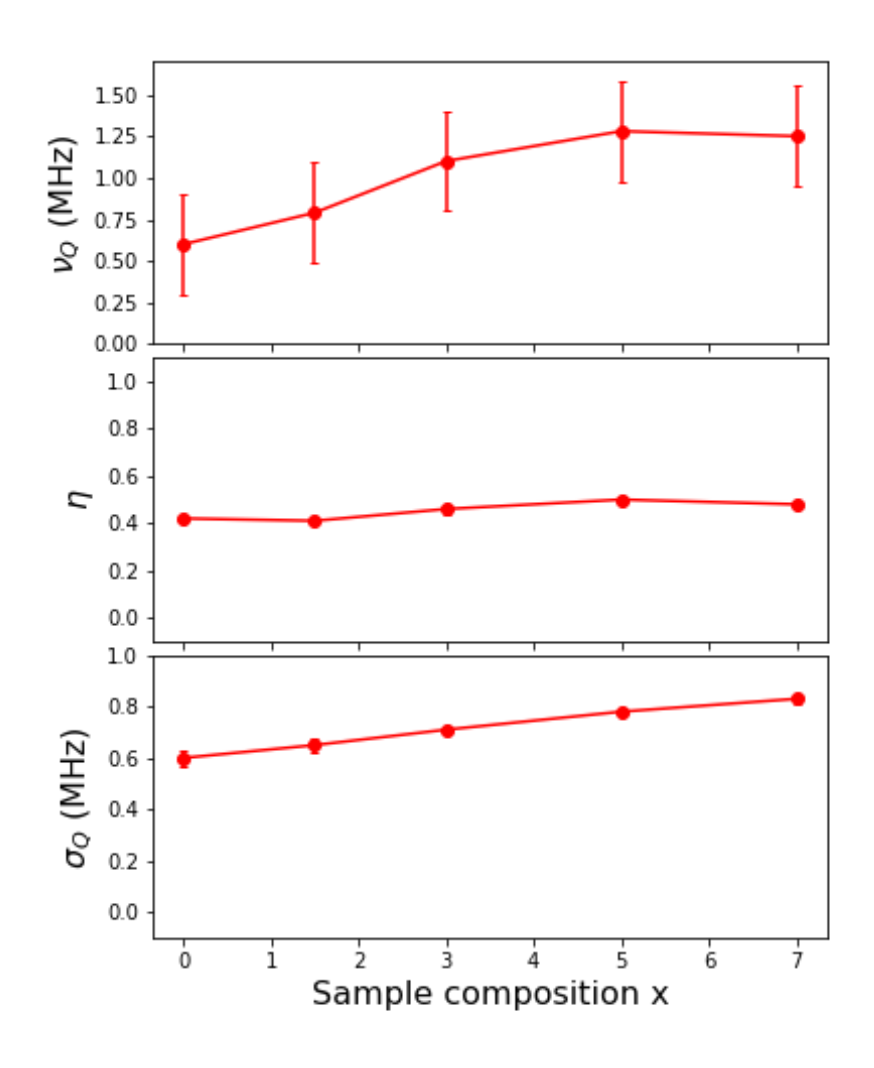


Figure 3. Electric field gradient parameters v_Q , η , and σ_Q at ²³Na sites, obtained for glasses Na₄P₂S_{7-x}O_x where x=0, 1.5, 3, 5, 7. The model assumes a Czjzek distribution of NMR powder patterns.

Figure 3 shows that the average v_{ϱ} value increases with increasing oxygen content, going from (0.6 ± 0.3) MHz at x = 0 to (1.3 ± 0.3) MHz at x = 5. In addition, η is non-zero, indicating that the average sodium site is not at a site of axial symmetry [9,11], and ranges from 0.41 to 0.50. Finally, σ_{ϱ} changes from 0.60 to 0.83 MHz across the composition range, a change of 38%, indicating that the distribution of EFG parameters $P(v_{\varrho}, \eta)$ is wider for glass compositions with higher oxygen content.

B. ²³Na central line NMR spectrum

The variation of the FWHM of the ²³Na resonance with temperature is due to the averaging effect of the fluctuating local fields resulting from ionic motion. The onset of motional narrowing occurs when the fluctuation frequency of the local field approaches the rigid lattice linewidth, and proceeds with increasing temperature until the linewidth is fully narrowed to the minimum determined by the inherent inhomogeneity of B₀.

Figure 4 shows the 23 Na NMR central line spectra for different temperatures of the x = 0 glass. The FWHM ranges from an average value of 4.7 kHz below 200 K to 0.8 kHz at 413 K. The FWHM was obtained by fitting the spectra to a Lorentzian function.

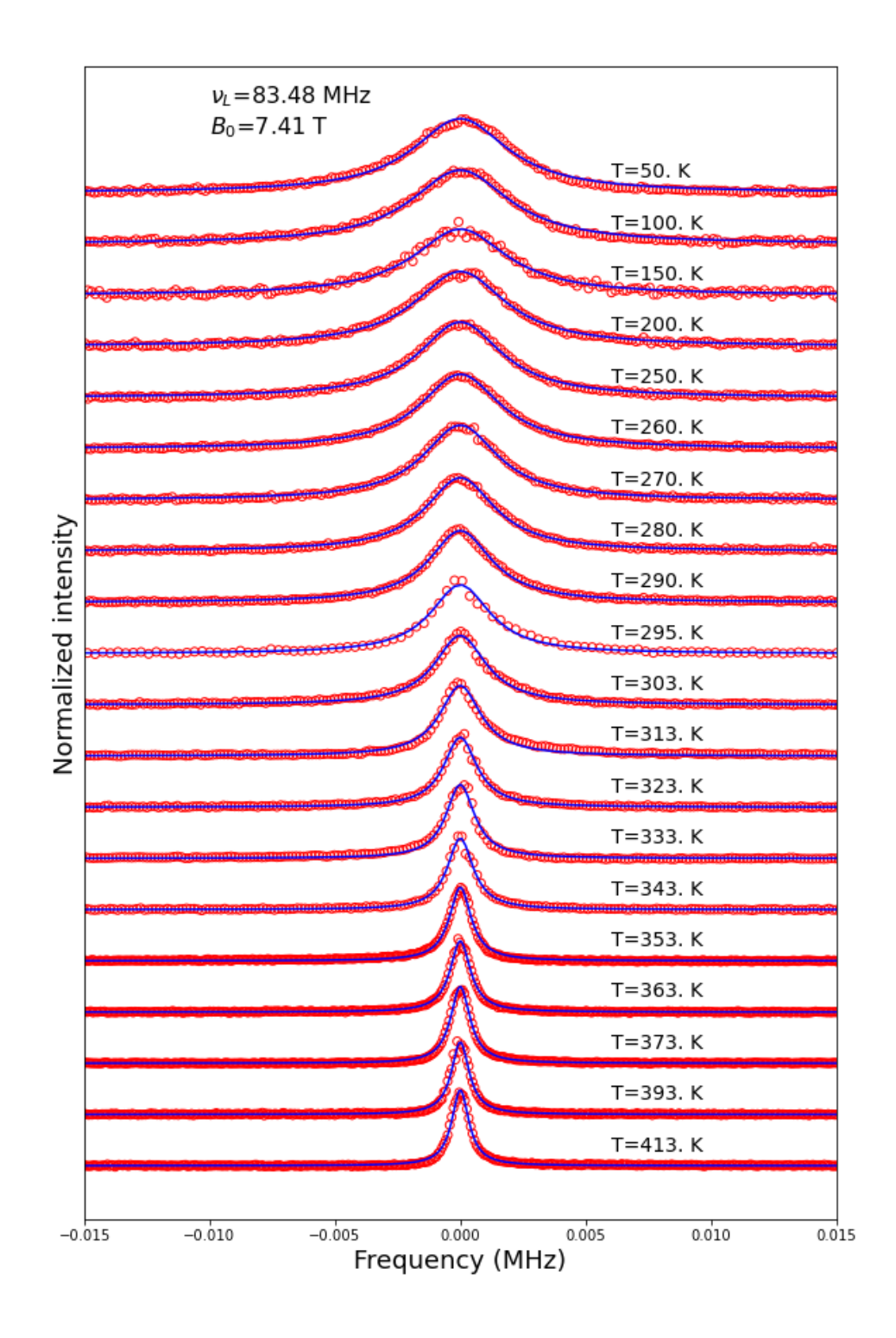


FIGURE 4. Temperature dependence of 23 Na NMR central line for Na₄P₂S_{7-x}O_x glass for x=0.0. The figure illustrates the motional narrowing of the NMR line with increasing temperature. The solid line shows a Lorentzian fit.

C. ²³Na central line spin-lattice relaxation

The nuclear spin-lattice relaxation time T_1 provides another probe of the timescale of nuclear motion. In glassy materials, the return to equilibrium of the nuclear spin magnetization $M_Z(t)$ is often well-described as a stretched exponential function. For saturation recovery experiments, the normalized magnetization is given by:

$$1-M_z(t)/M_{\infty} = \exp\left[-\left(\frac{t}{T_1}\right)^{\beta_z}\right]$$
 (1)

where the quantity β_Z characterizes the distribution of interaction strengths throughout the sample. Single exponential relaxation time behavior is a special case in which $\beta_Z = 1$. Figure 5 shows typical data, illustrated by select temperatures for the x = 0 sample. In this study both β_Z and T_1 were free parameters. Values for β_Z typically ranged from 0.6 at room temperature and approached 1 as temperature increased.

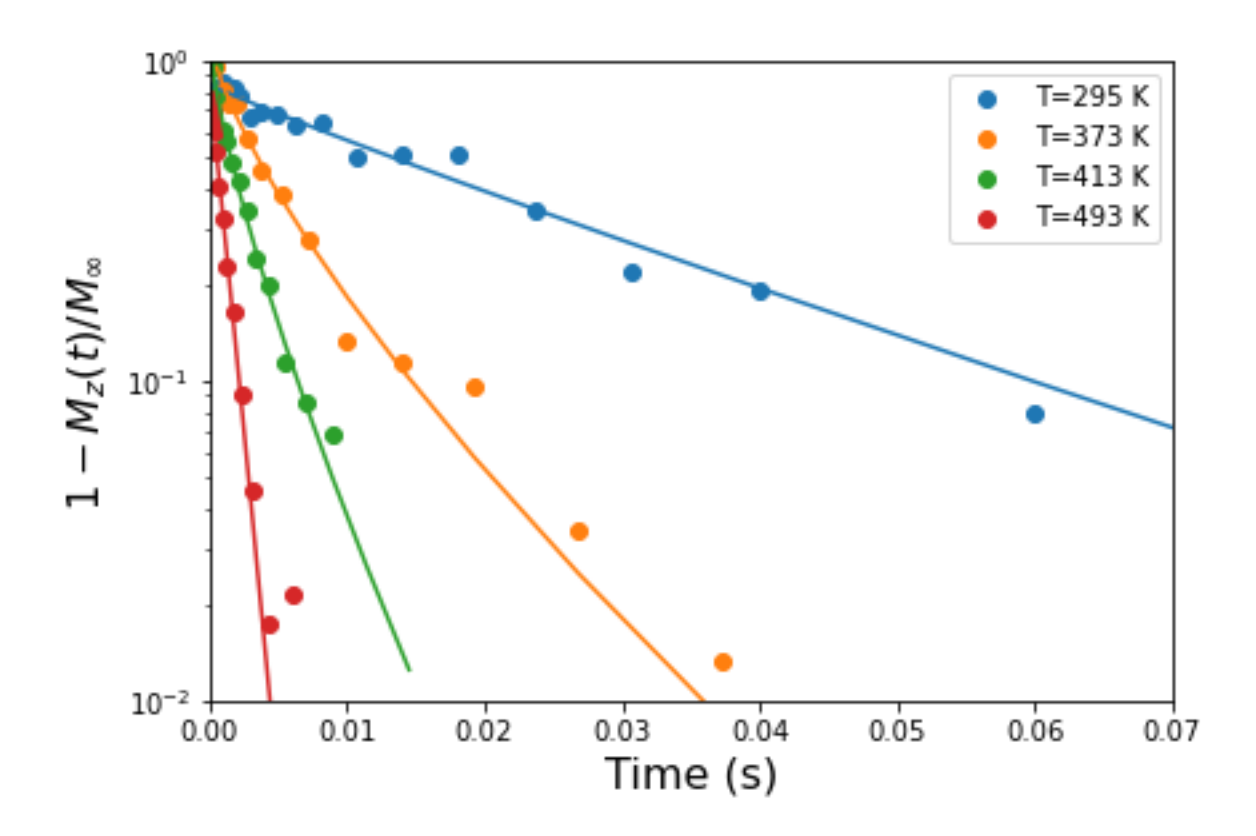


FIGURE 5. Example spin-lattice relaxation data of the 23 Na central line for the x = 0 glass Na₄P₂S₇.

FWHM and R_1 =1/ T_1 were measured for all samples, and the results are summarized in Fig. 6.

The FWHM data indicate a gradual increase in rigid-lattice linewidth as oxygen content increases. The onset of motional narrowing occurs at approximately 200 K for x=0 and 313 K for x=5. We do not include x=7 in the figure because we were unable to achieve appreciable line narrowing up to the glass transition temperature of the sample. We found only a 4% reduction in linewidth at the highest temperature. The onset temperature was found to be 410 \pm 20 K. This is consistent with the rather low Na⁺ ion conductivity of this pure oxide glass.

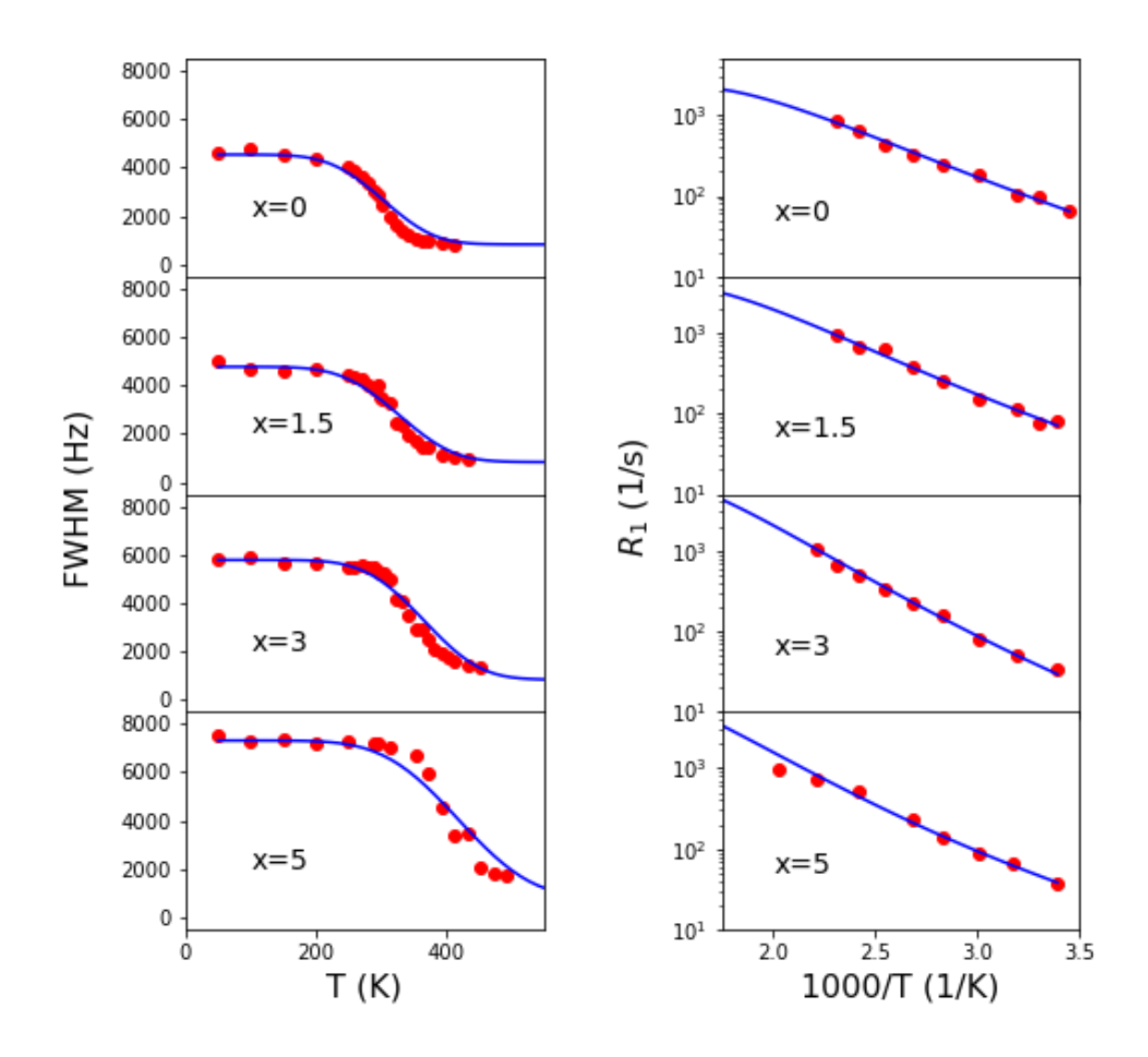


FIGURE 6. Temperature dependence of FWHM (left) and R_1 (right) for the 23 Na NMR central line for $Na_4P_2S_{7-x}O_x$ glassy solid electrolytes where x=0, 1.5, 3, 5. The solid lines were determined by simultaneously fitting line width and R_1 data as described in the text assuming a Gaussian distribution of activation barriers.

For temperatures below 200 K, a small but systematic increase in the linewidth occurs as temperature decreased. We observed this in other sodium glass samples, and

attribute the effect to trace quantities of a paramagnetic impurity. These have negligible effect on the high-temperature data, as shown in a previous study [17]. To remove this contribution, we fit the FWHM to a Curie law function A + B/T where A and B are constants, and then subtracted the contribution for all FWHM data. The results are shown in Fig. 6.

The theory of magnetic resonance predicts a maximum in R_1 when $\tau_C \omega_L = 1$, where τ_C is the autocorrelation time for nuclear motion, and ω_L is the Larmor frequency in rad/s. The relatively low glass transition temperatures T_g for this glass system, $T_g << 300$ °C, prevents reaching high enough temperatures to observe this effect before significant structural changes occur in the glass. The data therefore represent the slow motion regime for nuclear motion. In this regime, R_1 versus 1000/T on a semilog plot linearizes the data, and has a slope proportional to the activation energy ΔE_a .

D. ²³Na second moment

The magnetic dipole interaction between ²³Na nuclei depends on the internuclear separation r, and may therefore be used to investigate nuclear spatial distributions within the glass structure at temperatures where ionic motion is frozen out. However, because the ²³Na central line is determined by second order quadrupole interactions as well as magnetic dipole interactions, one must isolate the desired magnetic dipole interaction using a suitable method.

For sodium glasses, such a method has been proposed and implemented [12-14,25]. Homonuclear magnetic dipole and electric quadrupole interactions are bilinear in the nuclear spin z-component operator I_Z . Fluctuations in these interactions cannot be refocused by a Hahn echo pulse sequence ($\frac{\pi}{2}\Big|_{\chi} - \tau - \pi_y - \tau - echo$) and lead to irreversible reductions in the signal amplitude as a function of spin evolution time 2τ . For many materials, the spin-echo is characterized by a unique second moment M_2 and described by a Gaussian envelope:

$$\frac{I(2\tau)}{I_0} = exp\left(-\frac{M_2}{2}(2\tau)^2\right) \tag{2}$$

where $I(2\tau)$ is the echo amplitude as a function of evolution time. For glasses, a distribution of M_2 is more appropriate, and consequently Eqn. (2) does not describe $I(2\tau)$ well. One solution to this problem is to restrict data to short times, empirically determined to be in the approximate range of $100~\mu s < 2\tau < 250~\mu s$, and to then use successive Gaussian fits over a progressively smaller upper boundary time $2\tau_{max}$. The sequence of M_2 values may be extended to zero time using a linear extrapolation, to yield a short-time estimate of M_2 that should be sensitive to the closest—and therefore most strongly interacting—sodium nuclei [12]. We refer to this method as the zero-time M_2 method (ZTMM).

To reduce the sensitivity of ZTMM to high-frequency noise components, we used a model function to characterize the spin echo amplitude over the full time range. As has been seen in many glassy and disordered systems [22], a compressed exponential function may be used, and is given by:

$$\frac{I(2\tau)}{I_0} = exp\left(-\left(\frac{2\tau}{T_2}\right)^{\beta_{XY}}\right)$$
 (3)

where $1 < \beta_{\chi\gamma} < 2$. Figure 7(a) shows a typical $\frac{I(2\tau)}{I_0}$ and a fit to Eqn. (3). The fit describes the spin evolution very well over all time. Fig. 7(b) shows simulated data obtained by using the fit function to determine estimated values at short times. Following ZTMM, successive Gaussian fits are performed on the simulated data restricted to $2\tau_{min} < 2\tau < 2\tau_{max}$ over a progressively smaller upper boundary time $2\tau_{max}$. Fig. 7(c) shows the zero-time extrapolation. We refer to this method as the compressed exponential short-time extrapolation method (CESTEM). In order to account for the effect of different boundaries 2τ , and for different sampling densities, we performed CESTEM 10 times for each sample using randomly generated parameters consistent within the ranges: 0.1 ms $< 2\tau_{min} < 0.13$ ms, 0.2 ms $< 2\tau_{max} < 0.25$ ms, $8 < N_s < 12$, where N_s is the number of samples in the interval. These values were chosen based on experimental values used in previous studies .The M_2 values obtained were then averaged, and the standard deviation used as the error bar.

For systems in which interatomic distances r_{ij} are known, theory predicts an M_2 value for nuclear spin I = 3/2 given by [26]:

$$M_2 = 0.9562 \left(\frac{\mu_0}{4\pi}\right)^2 \gamma^4 h^2 \sum_{ij} r_{ij}^{-6}$$
 (4)

For crystalline systems where the structure is known, ZTMM and Eqn. (4) are in agreement to within 20% [13].

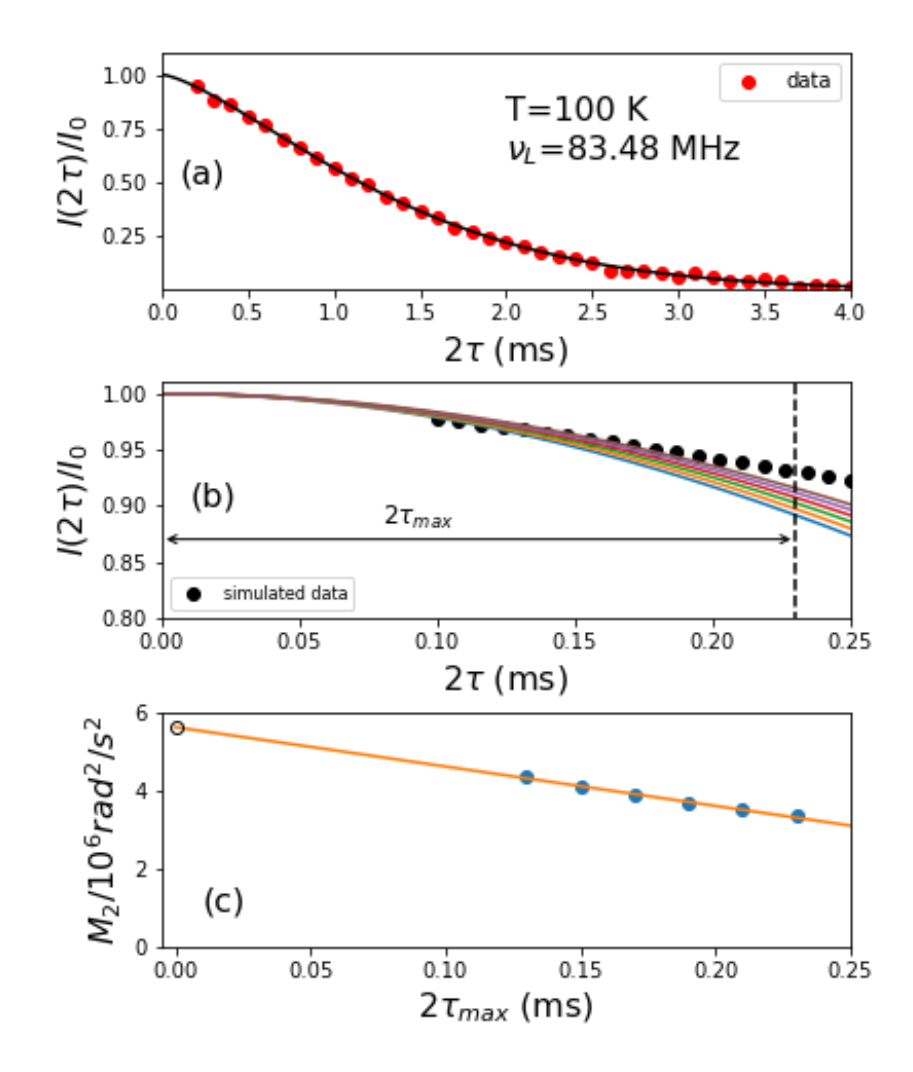


FIGURE 7. Compressed exponential short-time extrapolation method (CESTEM) for determining 23 Na central line second moment in the limit of short evolution times, illustrated for the Na₄P₂S_{7-x}O_x glass x=0. (a) The normalized spin-echo amplitude versus evolution time 2τ is shown (circles) for long times. The solid line shows a fit to the compressed exponential model discussed in the text. (b) Simulated data based on the model fit are then calculated over short times. These are fit to a Gaussian curve over a restricted values $2\tau_{min}$ (c) Successive short-time approximations to M_2 as a function of $2\tau_{max}$ are shown. Values are fit to a line and the y-intercept determines M_2 in the limit of zero evolution time, shown as an open circle. Data were obtained for T=100 K, B_0 =7.41 T and ν_L =83.48 MHz.

V. Discussion

A. ²³Na motional activation energies from FWHM and R₁ data

Following previous work [16,17], we modeled the 23 Na spin dynamics in the following way. As with many models of stochastic processes, the random nuclear hops were described by an exponential autocorrelation function with time constant τ_{∞} [27]. This correlation time was assumed to depend on motional activation energy ΔE_{act} according to the Arrhenius relation:

$$\tau_C(T) = \tau_{\infty} \exp\left(\frac{\Delta E_{act}}{k_B T}\right) \tag{5}$$

where τ_{∞} was fixed at 10^{-13} s for all calculations [16,17]. We found that single values of ΔE_{act} did not give satisfactory descriptions of data in our glass samples, and assumed a Gaussian distribution of activation energies (DAE) given by:

$$g(\Delta E_{act}) = \frac{1}{\sigma_E \sqrt{2\pi}} \exp\left(-\frac{(\Delta E_{act} - \Delta E_a)^2}{2\sigma_E^2}\right)$$
 (6)

The central line width due to motional narrowing resulting from ionic hopping through a glassy structure may be described by [9,16]

$$\delta\omega^{2} = \int_{0}^{\infty} d\Delta E_{act} g(\Delta E) \left[\delta\omega_{\infty}^{2} + \frac{2}{\pi} \left(\delta\omega_{0}^{2} - \delta\omega_{\infty}^{2} \right) \times \tan^{-1} \left(\tau_{C}(\Delta E_{act}) \cdot \sqrt{\delta\omega^{2}} \right) \right]$$
 (7)

where $\delta\omega_0^2$ and $\delta\omega_\infty^2$ represent the low- and high-temperature values of the second moment of the line width. These second moments were determined from the FWHM of Fig. 6. For

nuclear spin relaxation due to fluctuating electric quadrupole interactions resulting from ionic motion though a glass [16], the relaxation rate may be modeled as:

$$R_{1} = \frac{1}{T_{1}} = \frac{4\pi^{2} v_{Q}^{2}}{5} \left(1 + \frac{\eta^{2}}{3} \right) \int_{0}^{\infty} d\Delta E_{act} g(\Delta E_{act}) \left[\frac{\tau_{C}}{1 + (\tau_{C} \omega_{L})^{2}} + \frac{\tau_{C}}{1 + (2\tau_{C} \omega_{L})^{2}} \right]$$
(8)

where the quadrupole interaction parameters $v_{\it Q}$ and η were obtained from the average values in Fig. 3. Eqns. 5-8 form the NMR spin dynamics model for the glass.

The data of Fig. 6 were fit to this model with two free parameters, namely the mean barrier height for nuclear motion ΔE_a and the standard deviation of the energy barrier distribution σ_E . All others were found experimentally: the nuclear quadrupole parameters v_Q and η were determined experimentally from NMR field scans; $\delta \omega_0^2$ from the average of the low-temperature FWHM data of Fig. 6; and $\delta \omega_\infty^2$ as measured for sodium ions in aqueous solution.

Lines of fit are shown as solid lines in Fig. 6. The model describes both the FWHM and R_1 for all samples reasonably well.

Figure 8 shows the Gaussian DAE given by Eqn. (6) for the ΔE_a and σ_E obtained from the fits for each sample. The distributions have widths characterized by $\sigma_E = 0.1$ eV and average barrier heights ΔE_a that increase with oxygen content x.

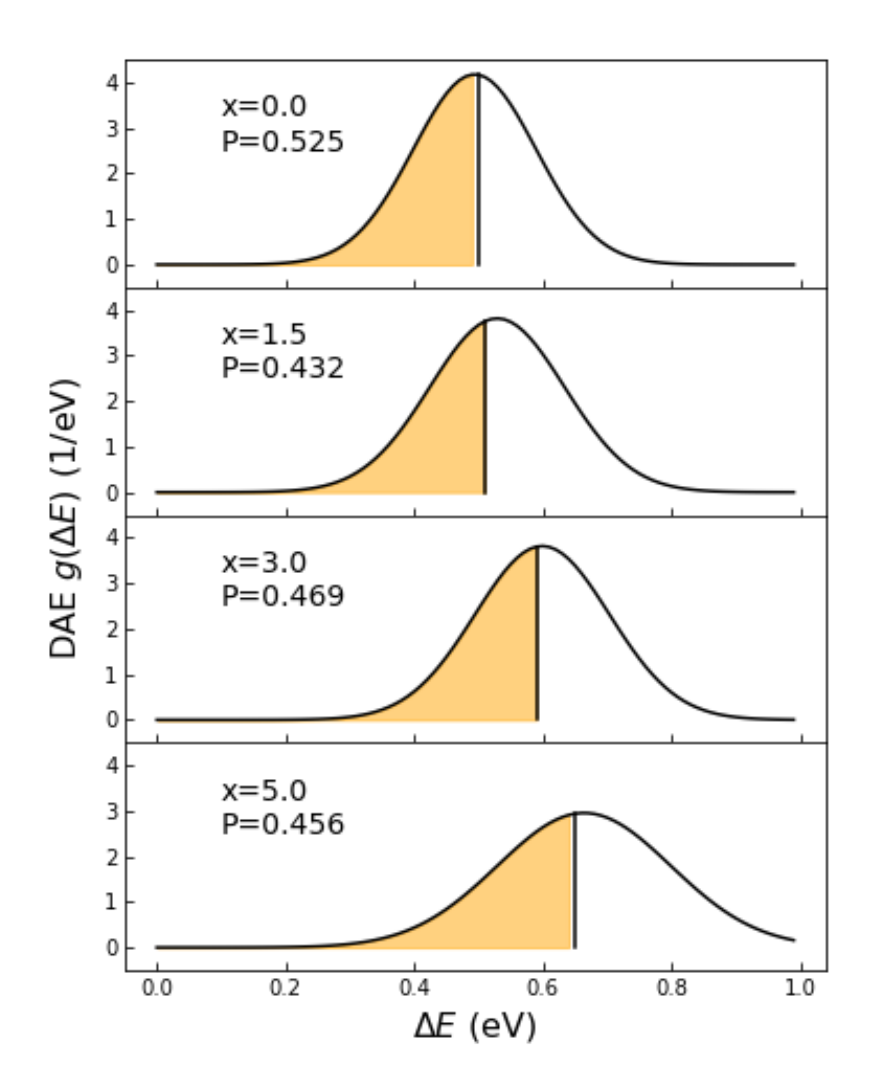


Figure 8. DAE for $Na_4P_2S_{7-x}O_x$ glasses for x=0, 1.5, 3, 5, obtained by fitting data of Fig. 6 to Eqns. 4-7. The vertical line indicates the activation energy determined by DC conductivity measurements [8]. The shaded area is interpreted as the critical percolation fraction P for the glass, and found from Eqn. (11b).

Figure 9 summarizes ΔE_a determined from NMR in this study, and DC conductivity data reported by [8]. In order to estimate ΔE_a by NMR for the x = 7 sample, the onset

temperature for motional narrowing was used to calculate an activation energy by the Waugh-Fedin method [28]:

$$\Delta E_{q-WF} = 1.62 \times 10^{-3} \, eV \, / \, K \times T_{onset}(K) \tag{9}$$

This resulted in a value of 0.66 ± 0.03 eV for the x=7 sample. Additionally, in order to estimate ΔE_a by DC conductivity for the x=7 sample, a parabolic fit was performed using the x=0 to 5 data and extrapolated, yielding $\Delta E_{a\text{-cond}}=0.63$ eV. (We show in Section E that a non-linear extrapolation can be justified based on a physical model of the ionic interaction.) These estimated ΔE_a values for x=7 are indicated as triangles in Fig. 9.

Figure 9 suggests $\Delta E_{a\text{-NMR}}$ values are generally higher than $\Delta E_{a\text{-cond}}$ values. This phenomenon has been reported in many systems [17-19,29]. The interpretation of this result is discussed in the next section.

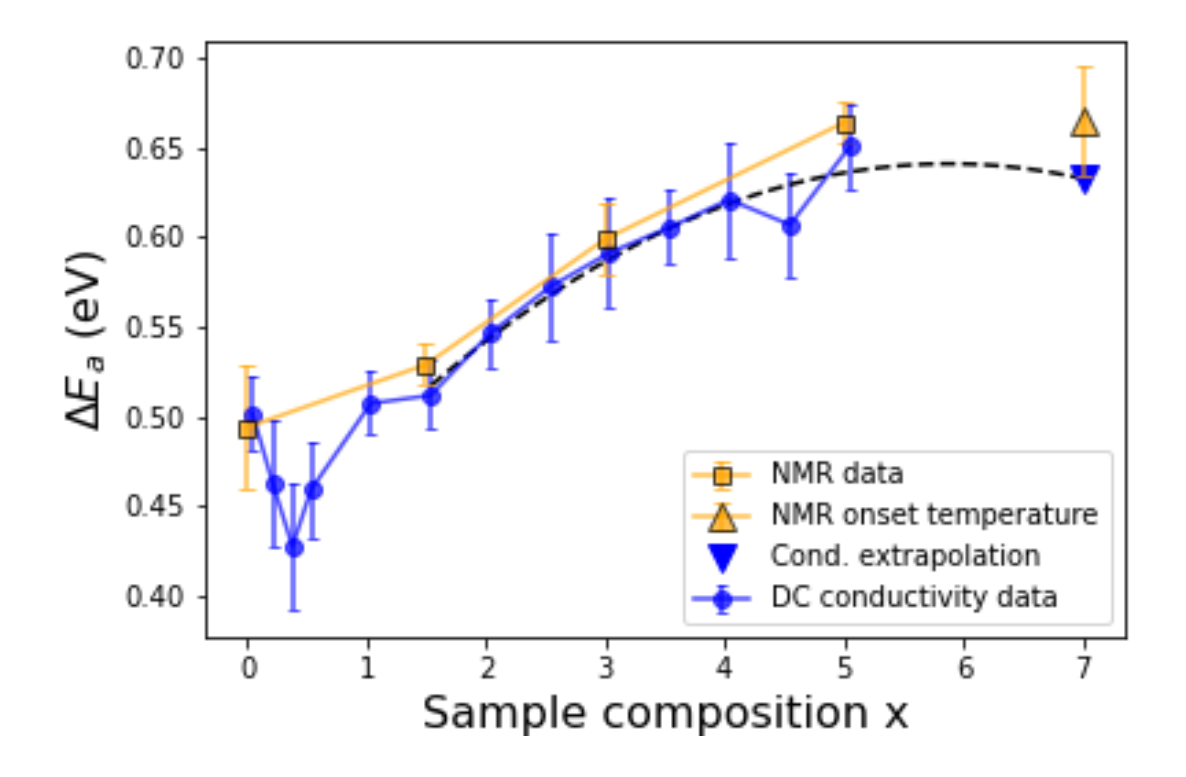


Figure 9. Activation energies for Na₄P₂S_{7-x}O_x glasses x= 0, 1.5, 3, 5 as determined by NMR (squares) and DC conductivity measurements (circles, Ref. [8]). The x=7 sample NMR ΔE_a was estimated by the onset temperature of motional narrowing using Eqn. (9) (triangle), and the DC conductivity ΔE_a (inverted triangle) by a parabolic extrapolation of the data, as indicated by the dashed line.

B. Percolation model

We viewed the ion dynamics detected by DC ionic conductivity in terms of a bond percolation model [30]. Ions in the glass are interconnected by a network of conduction pathways, each of which may be open to ion propagation, or closed to it. The average number of pathways per site is the Na-Na coordination number z. The minimum fraction of connected bonds needed for non-zero conduction is the critical percolation fraction P, and depends on z according to [30]:

$$P = \frac{1.45}{z}.$$
 (10)

This relationship is a near-invariant for percolation [30], and indicates that at the percolation threshold the average cation site sees approximately zP=1.5 unblocked pathways. Pathways above the activation energy threshold ΔE_p are considered blocked, and those below unblocked. This critical energy is taken to be the activation energy measured by DC conductivity $\Delta E_{a\text{-cond}}$ [19,29,31,32]:

$$\Delta E_{p} = \Delta E_{a-cond}$$
 (11a)

and satisfies [29]

$$P = \int_{0}^{\Delta E_{p}} g(\Delta E_{act}) d\Delta E_{act}$$
 (11b)

Eqn. (11b) is represented graphically in Fig. 8 as the shaded part of the curve, and the limit of integration ΔE_P is represented as a vertical line. Rearranging Eqns. (10) and (11), and using the Gaussian DAE of Fig. 8, one may find an expression for z:

$$z = \frac{2.90}{\left(1 - \operatorname{erf}\left(\frac{\Delta E_{a-\text{NMR}} - \Delta E_{a-\text{cond}}}{\sqrt{2}\sigma_E}\right)\right)}$$
(12)

where the error function is given by $\operatorname{erf}(x) = \sqrt{\frac{2}{\pi}} \int_{0}^{x} \exp(-t^{2}) dt$.

Figure 10 shows the result of applying Eqn. (12) to the data of Fig. 9. Error bars were determined by calculating the maximum and minimum values of z from Eqn. (12). The DAE σ_E values were taken from Fig. 8, and the uncertainties from Fig. 9.

Figure 10 gives the average number of paths for a mobile cation per site, as obtained from methods that probe ion dynamics. The result indicates consistency with face jumps through tetrahedral cages formed by anions, indicated as NaX_4 , for much of the composition range. For the x = 7 sample, the uncertainty is too large to make any decision about the preference for local geometry.

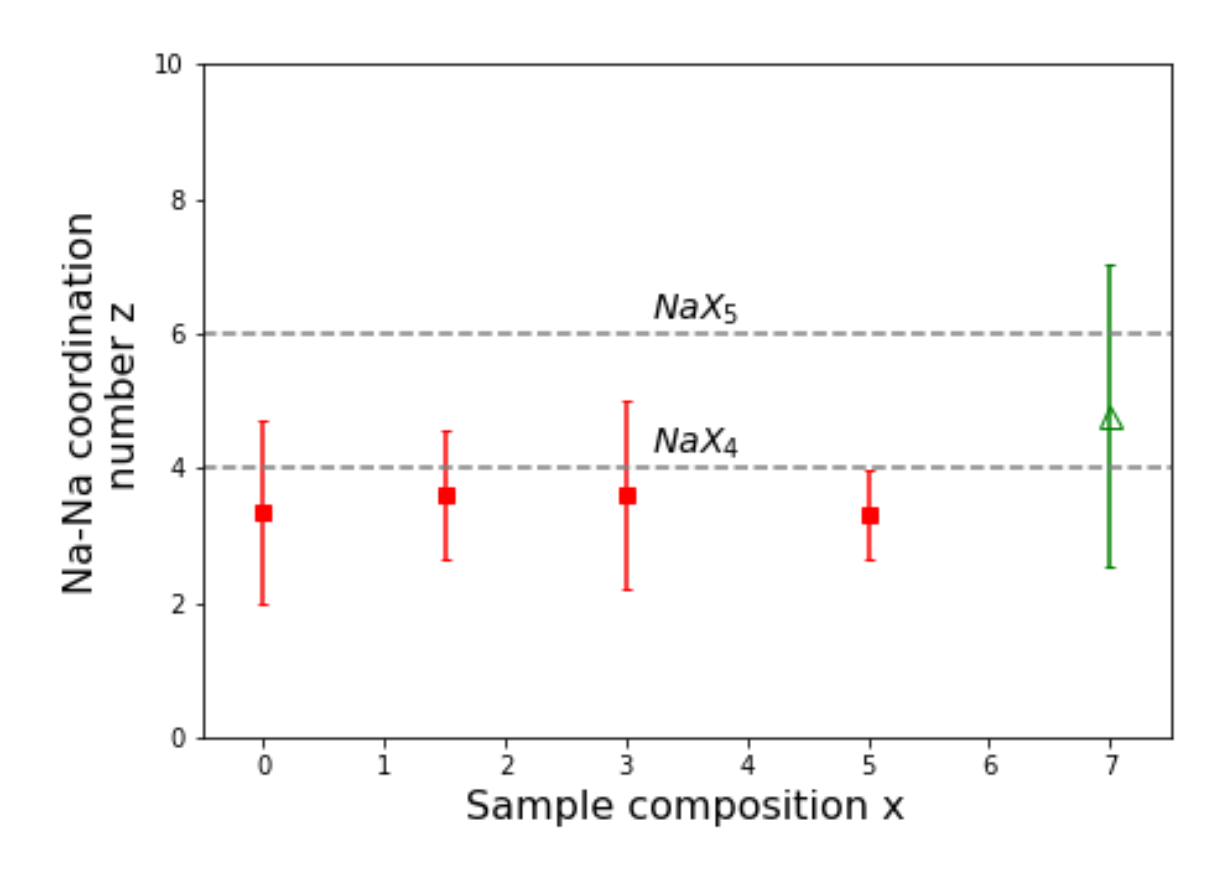


Figure 10. Sodium-sodium coordination number versus sample composition for $Na_4P_2S_{7-x}O_x$ glasses, x=0,1.5,3,5, (squares) as determined from Eqn. (12) based on experimental values

taken from Fig. 9. Dotted lines indicate the z expected for face-jumps through NaX₄ tetrahedral (4 faces) and NaX₅ trigonal bi-pyramidal (6 faces) sodium cages, where X=S, O.

D. Distribution of Na from M₂ measurements

Experimental M_2 values for the 23 Na magnetic dipole interaction were found, and are shown in Fig. 11 versus experimental values for sodium number density N, calculated from the density and molar mass of the glass [8]. These measurements are taken at a temperature (100 K) at which all ions are static, and thus part of the structural network.

In sodium glasses for which $N \le 1.5 \times 10^{28} \, \text{m}^{-3}$ [12], three functional forms of $M_2(N)$ have been reported: $\propto N^0$ (simple clustering, e. g. sodium silicate glass); $\propto N^1$ (random clustering distribution, e.g. sodium phosphate glass); and $\propto N^2$ (uniform distribution, e. g. sodium borate glass above $N \sim 1.3 \times 10^{28} \, \text{m}^{-3}$). In sodium invert glasses reported [17], $M_2(N) \propto N^2$ (yNa₂S+(1-y)[xSiS₂+(1-x)PS_{5/2}], where y = 0.50 and 0.67 and $1.3 \times 10^{28} \, \text{m}^{-3} \le N \le 1.8 \times 10^{28} \, \text{m}^{-3}$).

Reports have modeled the cation spatial distributions using computer simulations [12-14,33]. We give an overview of this approach and determine closed-form expressions that may be used to calculate M_2 , providing an alternative to simulations.

1) Of the behaviors discussed, simple clustering seems to be the least common in the studies reported, and has been suggested to be an indicator of ion conducting channels in the glass network [12]. In order to maintain constant ionic separation over the composition range, while N increases, could be explained by the ion

conducting channels that penetrate the glass network, as in a modified random network model [34]. Thus, modeling the details are complex, and will not be considered further here.

- 2) In the random clustering model, the lattice constant is fixed at a distance d_{min} , which represents the minimum separation distance between cations. Lattice sites are randomly populated by cations with probability $q = N/N_T$, where N_T is the cation number density for the total number of available lattice sites, and N is the number density N for the glass composition. If the model M_2 from Eqn. (4) is averaged over many trials, then $M_2 \propto q \cdot \sum_i r_i^{-6}$. The summation over internuclear distances is complicated for glasses since the long-range structure is an unsolved problem. Since bond lengths do not vary significantly between crystalline and glassy states, we performed the summation for two crystalline lattices in order to provide an understanding of the relation between M_2 and N. Because simple cubic (sc) structures have the lowest packing fraction of all crystalline systems, and hexagonal close packed (hcp) the highest, we performed numerical lattice sums for these structures. For these lattices, $N_T = d_{min}^{-3}$ (sc) and $1.41 d_{min}^{-3}$ (hcp), and substituting into Eqn. (4) one finds that $M_2(N) \propto N^1$, where the proportionality constant k is given in Table 1.
- 3) For the uniform distribution model, all cation locations are occupied, and the cation-cation separation r_{nn} changes to yield the number density for a given composition. For these lattices, the cation number densities are given by $N = r_{nn}^{-3}$ (sc)

and 1.41 r_{nn}^{-3} (hcp) . When the summation of Eqn. (4) is performed, one finds $M_2(N) \propto N^2$, where the proportionality constant k is given in Table 1.

In summary:

$$M_2^{\text{theory}}(N) = \begin{cases} k \cdot N^2, & \text{for uniform distribution} \\ k \cdot N, & \text{for random clustering distribution} \end{cases}$$
 (13)

	Uniform distribution	Random clustering distribution
Simple cubic (sc)	$k = C \cdot 8.40$	$k = C \cdot \frac{8.40}{d_{\min}^3}$
Hexagonal close packed (hcp)	k = C⋅7.37	$k = C \cdot \frac{10.2}{d_{\min}^3}$

Table 1. Multiplicative constant k in Eqn. (13) for different ion distribution models and crystal lattice types. Here $C=0.9562\left(\frac{\mu_0}{4\pi}\right)^2\gamma^4h^2$.

We plotted the uniform distribution models in Fig. 11 for both sc and hcp lattices. In order to determine an approximation for the random distribution, we noted that the glass modifiers Na₂X (X = S, O) have sc sodium lattices with lattice parameters 327 pm and 277 pm, respectively. We chose d_{min} =327 pm as a reasonable starting point. The models based on uniform sodium distribution are in better agreement with experiment than those for the random distributions (reduced χ^2 = 27 for uniform distribution, 556 for random distribution, using the average of sc and hcp as the model [35]). This behavior is similar to that observed in other invert glasses [17]. The implication is that these invert glasses form with the sodium ions seeking to maximize internuclear ²³Na distances at each composition.

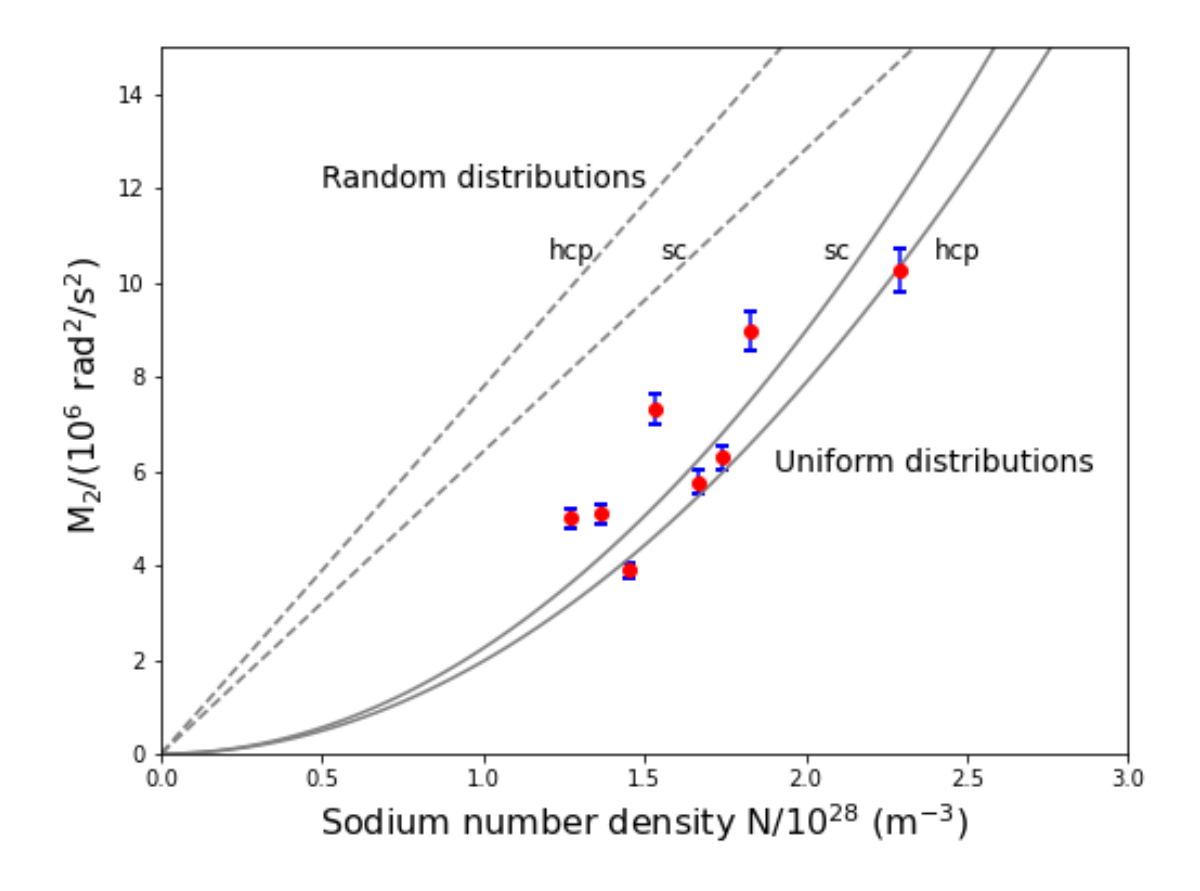


FIGURE 11. Second moment of Na-Na magnetic dipole interaction versus sodium number density for $Na_4P_2S_{7-x}O_x$ glasses for x=0, 1.5, 2.5, 3, 4, 4.5, 5, 7. Number density increases with increasing x. Solid lines (uniform distribution) and dotted lines (random distribution) were calculated by Eqn. (13) and Table 1. Random distribution values were calculated using $d_{min}=327$ pm, the sodium-sodium separation for glass modifier Na_2S . See text for details.

E. Model for activation energy

From the previous section, given the uniform distribution of sodium in this system, the average sodium-sodium distance $\lambda(x)$ may be estimated as:

$$\lambda(x) = \left(\kappa \frac{1}{N(x)}\right)^{1/3} \tag{14}$$

where $\kappa=$ constant that depends on the sublattice geometry (1 for sc, $\sqrt{2}$ for hcp), and N(x) is the sodium number density.

We modeled the activation energy using the CMAS model [36]. In order for the Na to jump, it must overcome the Coulombic binding energy of the X anion, and strain the lattice as it dilates the structural opening through which it moves. The total activation energy is then:

$$\Delta E_{act} = \Delta E_C + \Delta E_S \tag{15}$$

Parameters necessary for calculating the Coulombic contribution to the activation energy are indicated in Fig. 12.

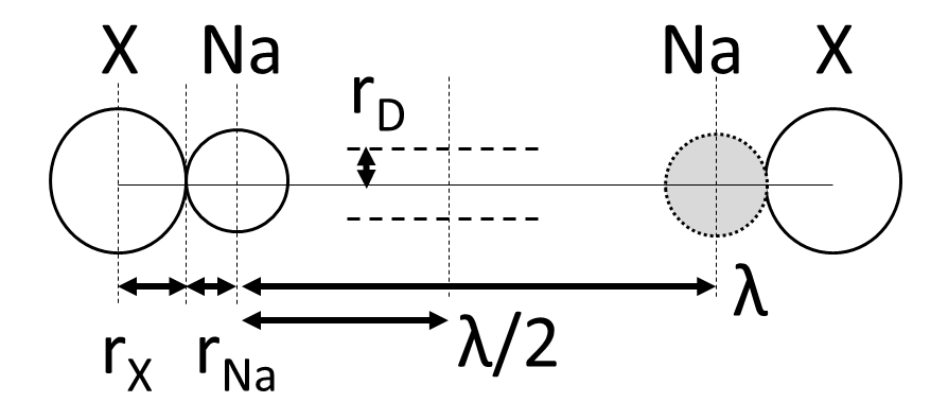


FIGURE 12. Diagram of relevant quantities needed for estimating the Coulombic contribution in the CMAS model. The sodium and anion X radii are indicated, as well as the average jump distance λ from one sodium site to another. The shaded circle indicates an unoccupied sodium site to which the sodium cation can jump.

The Coulombic contribution is defined as the energy difference between the sodium-anion (X) interaction at ion separations of $r_{\rm X}(x)+r_{\rm Na}$ and $r_{\rm X}(x)+r_{\rm Na}+\lambda/2$ yielding:

$$\Delta E_{C} = M_{C} \frac{k_{e} Z_{Na} Z_{X} e^{2}}{\varepsilon_{\infty}} \left(\frac{1}{r_{X} + r_{Na}} - \frac{1}{r_{X} + r_{Na} + \lambda/2} \right)$$
(16)

where

 k_e = Coulomb's constant, $Z_{Na,X}$ =

magnitude of Na, X charge in units of electron charge (both 1), $r_{Na} =$ sodium ionic radius (1.02 Å [37]), $r_X =$ average anionic radius, $\lambda =$ sodium – sodium separation, $\epsilon_{\infty} =$ dielectric constant. The Madelung constant M_C may be interpreted

as the correction factor that adjusts the Coulomb interaction for a single model site to include the all the Coulomb interactions throughout the glass. Though in principle each glass composition would have a unique M_C , we assumed a single average value across the entire glass composition and used this as an adjustable parameter. Finally, in this oxy-sulfide system the average anion radius is taken to be the number-weighted average of sulfur and oxygen anions:

$$\mathbf{r}_{\mathbf{x}}(\mathbf{x}) = \left(\frac{\mathbf{x}}{7}\right) \mathbf{r}_{\mathbf{0}} + \left(\frac{7 - \mathbf{x}}{7}\right) \mathbf{r}_{\mathbf{S}} \tag{17}$$

where $r_S = 1.84$ Å, $r_O = 1.23$ Å [37]. The dielectric constants were obtained from [8]. In general, the strain contribution to the activation energy is given by [38]

$$\Delta E_{S} = \pi G(x) \frac{\lambda}{2} (r_{Na} - r_{D})^{2}$$
(18)

where G(x) is shear modulus, $r_D = doorway$ radius, the opening size available to the sodium ion for motion through the glass. However, calculations for these materials show that the strain energy is at most 3% of the overall activation energy [8]. For this reason, we will ignore the strain energy contribution and consider only the Coulombic part.

Figure 13 shows model activation energies calculated using Eqn. (16). The dotted lines indicate estimates for two M_C value chosen to bracket the data. The model follows the main trends in the data. In the range $0 \le x \le 5$, the CMAS model shows ΔE_{act} increases monotonically. Differences between the model and data may be due in part to the simplifying assumption that all glasses possess the same nominal M_C value. For sc lattice in Eqn. (14),

 M_C =2.65±0.15 , and for hcp M_C =2.5±0.1. These values are similar to those found in other sodium glasses [17,36].

In the region $5 \le x \le 7$, ΔE_{act} shows non-linear behavior. This provides support for the parabolic extrapolation procedure that was applied in Section A.

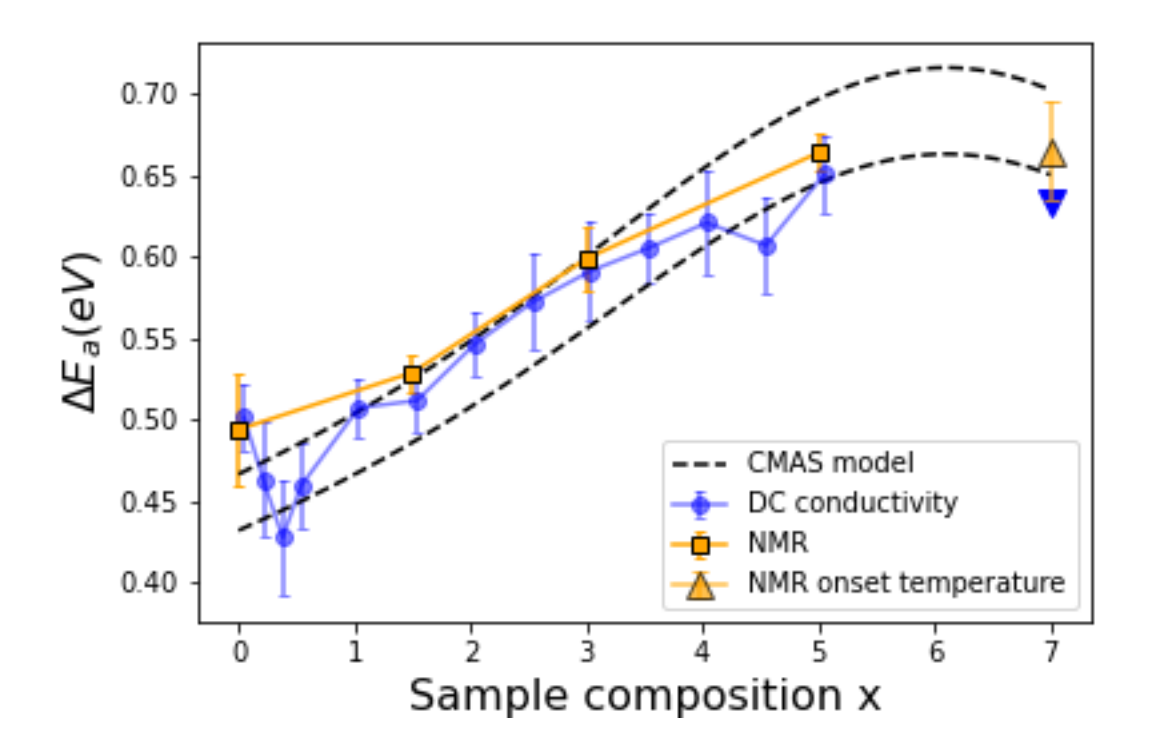


FIGURE 13. Activation energy data for $Na_4P_2S_{7-x}O_x$ glasses from Fig. 9 compared with values calculated from the CMAS model. Dotted lines show Coulomb interaction term (Eqn. (16)) for simple cubic sublattice model, where Madelung constant $M_C = 2.5$ (lower) and 2.7 (upper).

F. Summary

From estimate of the critical percolation fraction P and Na – Na coordination number z, one can estimate the fraction of static cations. The probability of a blocked bond is (1 - P), and the probability of n out of z blocked bonds is described by a binomial distribution

 $\binom{z}{n}(1-P)^nP^{z-n}$. Taking z=4 for the samples for $x\leq 5$ (Fig. 10), which occurs for face jumps through NaX4 cages, the probability of 4 blocked sites (static cation for purposes of ionic conduction) ranges from 5-10%. Thus, most cations are available to participate in ionic conduction. The activation energy to motion is described reasonably well by Coulombic interaction between the cation and the cage formed by the anions, as described by the CMAS model. As sulfur is replaced by oxygen, and the cages become smaller, the model accounts for an increase in activation energy, taking into account the broader ionic interactions in the glass by a multiplicative Madelung constant. Thus, while the uniform distribution of the cations suggests the effect of cation – cation repulsion, the CMAS model indicates that the dominant effect is due to the anionic cage. However, the model does not show a local minimum in activation energy at low x concentrations as suggested by the DC conductivity data.

VI. Conclusions

We presented a 23 Na nuclear spin dynamics model for interpreting NMR spin-lattice relaxation and central linewidth data in the invert glass system Na₄P₂S_{7-x}O_x , $0 \le x \le 7$. Assuming a Gaussian DAE, the average and standard deviation of the activation energy for ionic motion was determined across the glass composition. A consistent difference between the activation energies determined by NMR and DC conductivity measurements was observed, and interpreted using a percolation theory model. From this, the Na-Na

coordination number of the sodium sublattice was obtained. These values were consistent with the hypothesized values resulting from the geometries of sodium cages that form in these glasses, with the predominant mode for sodium jumps through faces of the structures. We determined the NMR second moment M_2 resulting from the Na-Na magnetic dipole interaction of nearest neighbors. Values obtained as a function of sodium number density $M_2(N)$ were in agreement with crystalline models for uniform distributions. A simple Coulombic attraction model between sodium cation and X anion was applied to calculate the activation, and demonstrated an increase in activation energy with increasing oxygen content x, consistent with the data for $1.5 \le x \le 7$. For small oxygen concentrations $0 \le x \le 1.5$, however, the model was not consistent with a local minimum in activation energy as suggested by DC conductivity data.

VII. Appendix

A ²³Na nucleus (I=3/2) can be described by a nuclear spin Hamiltonian [9,11]

$$\mathcal{H} = \mathcal{H}_{Z} + \mathcal{H}_{O} + \mathcal{H}_{D} \tag{19}$$

where the Zeeman term $\mathcal{H}_{Z}=-\gamma h B_{0}I_{z}$ is the interaction of the nuclear spin with the external magnetic field B_0 ; the quadrupole term $\mathcal{H}_{\mathcal{Q}} = \frac{e^2q\mathcal{Q}}{4I(2I-1)}[(3I_z^2-I^2)+(\frac{\eta}{2})(I_+^2+I_-^2)]$ describes the electric quadrupole interaction with the local electric field gradient $V_{ij} = \partial^2 V / \partial x_i \partial x_j$; and the magnetic dipole term $\mathcal{H}_{\!\scriptscriptstyle D}$ is the magnetic dipole-dipole interaction between nuclear spins. Here \mathcal{H}_{o} is written in the principal axis system (PAS) of the electric field gradient tensor, and the PAS axes are defined such that $|V_{ZZ}| \ge |V_{YY}| \ge |V_{XX}|$. The quantity eQ is the quadrupole moment of the $^{23}\mathrm{Na}$ nucleus, $eq=\left|V_{ZZ}\right|$, the quadrupole frequency $\nu_{\mathcal{Q}}=\frac{3e^2q\mathcal{Q}}{2I(2I-1)h}$, and asymmetry parameter $\eta = \frac{V_{XX} - V_{YY}}{V_{ZZ}}$. The conditions of this study, namely $\mathcal{H}_Z > \mathcal{H}_Q$, result in a spectrum with a sharp central transition line ($I_z=-1/2\leftrightarrow 1/2$) flanked by one satellite peak on either side ($I_z=1/2\leftrightarrow 3/2$ and $-1/2\leftrightarrow -3/2$). For a single crystal, this results in a central line symmetrically straddled by two quadrupole satellites, with separation proportional to v_o . For a crystalline powder, the distribution in grain orientations results in features (singularities and shoulders) that may be exploited to extract a unique $v_{\mathcal{Q}}$ and η for each non-equivalent resonant nuclear site in the crystal [23].

For glasses, a distribution of local environments exists due to variations in bond angle and bond length in the system. We modeled the powder patterns in a manner similar to

work in other sodium glasses [17]. If $f_{crystal}(\nu_Q, \eta)$ is the normalized crystalline powder pattern for a single local environment characterized by ν_Q and η , and $P(\nu_Q, \eta)$ represents the distribution function for ν_Q and η arising from the variation in local environments, then the powder pattern for the glass is given by the weighted sum:

$$f_{glass}(v_{Q}, \eta) = \sum_{v_{Q}, \eta} f_{crystal}(v_{Q}, \eta) P(v_{Q}, \eta)$$
(20)

In previous work, we obtained satisfactory results with $P(v_Q,\eta)$ given by the product of two independent Gaussian distributions, one each for v_Q and . However, the electric field gradients in the x, y, and z directions—and therefore v_Q and η —are correlated, and thus not independent. We have here chosen to use the Czjzek distribution, which describes the distribution of v_Q and η in a single function, and which arises in amorphous solids [24]. The distribution is given by:

$$P(\nu_{Q}, \eta) = \frac{1}{\sqrt{2\pi}\sigma_{Q}^{5}} \nu_{Q}^{4} \cdot \eta \cdot \left(1 - \frac{\eta^{2}}{9}\right) \cdot \exp\left(-\frac{\nu_{Q}^{2}\left(1 + \frac{\eta^{2}}{3}\right)}{2\sigma_{Q}^{2}}\right)$$
(21)

The quantity $\sigma_{\scriptscriptstyle \mathcal{Q}}$ parameterizes the width of the distribution.

Acknowledgments

Funding for this work was provided by the ARPA-E of the Department of Energy through contract number DE-AR0000654 and DE-AR-0000778. Additional funding for this work was provided by the Vehicle Technology Office within the Department of Energy though the contract DE-EE0008852, the Iowa Energy Center of the Iowa Department of Economic Development through grant number 307352 and by the National Science Foundation through grant DMR 1936913. In addition, support came from the U.S. Department of Energy, Office of Basic Energy Sciences, Division of Materials Sciences and Engineering. Ames Laboratory is operated for the U.S. Department of Energy by Iowa State University under Contract No. DEAC02-07CH11358. A. Shastri and N. Rons are grateful to the DOE for the opportunity to participate in the Summer 2021 Ames Lab Visiting Faculty Program, through which parts of this project were performed.

Reference List

- [1] Y. Zhao, K.R. Adair, X. Sun, Recent developments and insights into the understanding of Na metal anodes for Na-metal batteries, Energy & Environmental Science. 11 (2018) 2673-2695.
- [2] C.A. ANGELL, Oxide Glasses in Light of the "Ideal Glass" Concept: I, Ideal and Nonideal Transitions, and Departures from Ideality*, J Am Ceram Soc. 51 (1968) 117-124.
- [3] S.W. Martin, Glass and Glass-Ceramic Sulfide and Oxy-Sulfide Solid Electrolytes, in: Anonymous Handbook of Solid State Batteries, WORLD SCIENTIFIC, 2015, pp. 433-501.
- [4] A.K. Varshneya, J.C. Mauro, Fundamentals of Inorganic Glass, Third Edition ed., Elsevier, Cambridge, MA, USA, 2019.
- [5] A. Hayashi, K. Noi, A. Sakuda, M. Tatsumisago, Superionic glass-ceramic electrolytes for room-temperature rechargeable sodium batteries, Nature Communications. 3 (2012) 856.
- [6] Y. Kim, J. Saienga, S.W. Martin, Anomalous Ionic Conductivity Increase in Li₂S + GeS₂ + GeO₂ Glasses, J Phys Chem B. 110 (2006) 16318-16325.
- [7] S. Kmiec, A. Joyce, D. Bayko, S.W. Martin, Glass formation and structure of melt quenched mixed oxy-sulfide Na4P2S7-xOx glasses for $0 \le x \le 5$, J. Non Cryst. Solids. 534 (2020) 119776.
- [8] S.J. Kmiec, Development of sodium ion conducting mixed anion glassy solid-state electrolytes, (2020).
- [9] A. Abragam, Principles of Nuclear Magnetism, Clarendon Press, Oxford, 1989.
- [10] M.H. Levitt, Spin Dynamics: Basics of Nuclear Magnetic Resonance, 2nd ed., John Wiley & Sons, Chichester, England; Hoboken, NJ, 2008.
- [11] C.P. Slichter, Principles of Magnetic Resonance, Springer-Verlag, New York, 1990.
- [12] H. Eckert, Short and Medium Range Order in Ion-Conducting Glasses Studied by Modern Solid State NMR Techniques, Zeitschrift fuer Physikalische Chemie. 224 (2010) 1591.
- [13] B. Gee, H. Eckert, ²³Na nuclear magnetic resonance spin echo decay spectroscopy of sodium silicate glasses and crystalline model compounds, Solid State Nuclear Magnetic Resonance. 5 (1995) 113-122.
- [14] E. Ratai, M. Janssen, H. Eckert, Spatial distributions and chemical environments of cations in single- and mixed alkali borate glasses: Evidence from solid state NMR, Solid State Ionics. 105 (1998) 25-37.

- [15] D. Larink, H. Eckert, S.W. Martin, Structure and Ionic Conductivity in the Mixed-Network Former Chalcogenide Glass System $[Na_2S]_{2/3}[(B_2S_3)_x(P_2S_5)_{1-x}]_{1/3}$, J. Phys. Chem. C. 116 (2012) 22698-22710.
- [16] M. Storek, M. Adjei-Acheamfour, R. Christensen, S.W. Martin, R. Boehmer, Positive and Negative Mixed Glass Former Effects in Sodium Borosilicate and Borophosphate Glasses Studied by ²³Na NMR, The Journal of Physical Chemistry B. 120 (2016) 4482-4495.
- [17] A. Shastri, D. Watson, Q. Ding, Y. Furukawa, S.W. Martin, 23 Na nuclear magnetic resonance study of yNa₂S + $(1 y)[xSiS_2 + (1 x)PS_{5/2}]$ glassy solid electrolytes, Solid State Ionics. 340 (2019) 115013.
- [18] I. Svare, F. Borsa, D.R. Torgeson, S.W. Martin, Connection between NMR relaxation and electrical conductivity from distributions of activation energies of ionic motion in some fast-ion conductors, Journal of Non-Crystalline Solids. 172 (1994) 1300-1305.
- [19] I. Svare, F. Borsa, D.R. Torgeson, S.W. Martin, Correlation functions for ionic motion from NMR relaxation and electrical conductivity in the glassy fast-ion conductor (Li₂S)_{0.56}(SiS₂)_{0.44}, Phys.Rev.B. 48 (1993) 9336-9344.
- [20] A. Narath, Nuclear Spin-Lattice Relaxation in Hexagonal Transition Metals: Titanium, Phys.Rev. 162 (1967) 320-332.
- [21] E. Fukushima, S.B.W. Roeder, Experimental Pulse NMR: A Nuts and Bolts Approach, Addison-Wesely Publishing Company, Inc., Reading, Massachusetts, 1981.
- [22] E.W. Hansen, X. Gong, Q. Chen, Compressed Exponential Response Function Arising From a Continuous Distribution of Gaussian Decays Distribution Characteristics, Macromol. Chem. Phys. 214 (2013) 844-852.
- [23] M. H. Cohen, F. Reif, Quadrupole Effects in Nuclear Magnetic Resonance Studies of Solids, in Solid State Physics, in: D.T. F. Seitz (Ed.), Academic Press, New York, 1957, pp. 321-438.
- [24] G. Czjzek, J. Fink, F. G\otz, H. Schmidt, J.M.D. Coey, J.-. Rebouillat, A. Li\'enard, Atomic coordination and the distribution of electric field gradients in amorphous solids, Phys.Rev.B. 23 (1981) 2513-2530.
- [25] D. Larink, H. Eckert, M. Reichert, S.W. Martin, Mixed Network Former Effect in Ion-Conducting Alkali Borophosphate Glasses: Structure/Property Correlations in the System $[M_2O]_{1/3}(B_2O_3)_x(P_2O_5)_{1-x}]_{2/3}$ (M = Li, K, Cs), J. Phys. Chem. C. 116 (2012) 26162-26176.
- [26] J. Haase, E. Oldfield, Spin-Echo Behavior of Nonintegral-Spin Quadrupolar Nuclei in Inorganic Solids, J. Magn. Reson. Series A. 101 (1993) 30.

- [27] N. Bloembergen, E.M. Purcell, R.V. Pound, Relaxation Effects in Nuclear Magnetic Resonance Absorption, Phys. Rev. 73 (1948) 679.
- [28] J.S. Waugh, I. Fedin, Soviet Physics Solid State. 4 (1963) 1633.
- [29] I. Svare, Conductivity and NMR relaxation from ionic motion in disordered glasses with distributions of barriers, Solid State Ionics. 125 (1999) 47-53.
- [30] R. Zallen, The Physics of Amorphous Solids, John Wiley and Sons, Weinheim, Federal Republic of Germany, 2004.
- [31] I. Svare, S.W. Martin, F. Borsa, Stretched exponentials with T-dependent exponents from fixed distributions of energy barriers for relaxation times in fast-ion conductors, Phys. Rev. B. 61 (2000) 228-233.
- [32] S.W. Martin, F. Borsa, I. Svare, Proc. Electrochem. Soc. 2000-32 (2001) 66.
- [33] J. Dirk Epping, W. Strojek, H. Eckert, Cation environments and spatial distribution in Na₂O-B₂O₃ glasses: New results from solid state NMR, Phys. Chem. Chem. Phys. 7 (2005) 2384-2389.
- [34] G.N. Greaves, S.J. Gurman, C.R.A. Catlow, A.V. Chadwick, S. Houde-Walter, C.M.B. Henderson, B.R. Dobson, A structural basis for ionic diffusion in oxide glasses, Philos. Mag. A. 64 (1991) 1059-1072.
- [35] P.R. Bevington, Data Reduction and Error Analysis for the Physical Sciences, McGraw-Hill, New York, 1969.
- [36] S.W. Martin, C. Bischoff, K. Schuller, Composition Dependence of the Na+ Ion Conductivity in 0.5Na2S + 0.5[xGeS2 + (1 x)PS5/2] Mixed Glass Former Glasses: A Structural Interpretation of a Negative Mixed Glass Former Effect, J Phys Chem B. 119 (2015) 15738-15751.
- [37] R.D. Shannon, Revised effective ionic radii and systematic studies of interatomic distances in halides and chalcogenides, Acta Cryst. A32 (1976) 751-767.
- [38] D. McElfresh, D.G. Howitt, Activation Enthalpy for Diffusion in Glass, J Am Ceram Soc. 69 (1986) C-237-C-238.